Supporting Information

Interaction between Single Noble Metal Atom and Graphene Edge: A Study via Aberration-corrected Transmission Electron Microscopy

METHODS

Preparing Monolayer Graphene with Free Edges. Single-layer graphene was grown on a 25 μm-thick copper foil in a flow-type low pressure reactor.[1] The transferring procedure was as follows:[2] (1) float the graphene-coated copper foil on the surface of 0.2 M $FeCl_3$ solution; (2) place the TEM grid (Protochips®) onto the foil with the carbon-coated side facedown; (3) after completely dissolving the copper, the grid is rinsed with DI water and dried with a filter paper.

The defect generation was realized in a pulsed laser deposition (PLD) chamber with a background pressure of 10^{-8} Torr. The transferred graphene on TEM grid was placed in the up straight position to the target with a distance of 100 mm. A pulsed high-power laser (400 mJ/pulse and 40 ns/pulse) is used to eject particles from the target surface, which bombard the free-standing graphene. The bombarded graphene layer has holes with various sizes and is free of contamination. Then the noble metal Pt and Au are deposited for a nominal thickness of ~1Å using a sputtering tool.

Transmission Electron Microscopy. TEM imaging is carried out using an aberration-corrected and monochromated FEI Titan 80-300 microscope with a typical electron beam current density of about 7×106 $e•s^{-1}•nm^{-2}$ (100 A/cm2). The third-order spherical aberration is carefully tuned to about 1 μm. The microscope was operated at 60 kV in order to minimize the knock-on

damage to graphene. Since the point resolution and the information limit are more sensitive to the chromatic aberration at lower operation voltage, the gun monochromator has been excited to 1.8 so as to reduce the electron energy spread to < 0.15 eV. Images are recorded on a charge coupled device (CCD) camera (2 k × 2 k, Gatan UltraScanTM 1000) with mode of binning two. The read-out time is 0.5 s. The HRTEM images are taken with an exposure time of 2 s and a spatial sampling of 0.20 Å / pixel.

HRTEM image simulations have been performed using the commercial software MacTempas. The input microscope parameters are: an acceleration voltage of 60 kV, a spherical aberration of 1 μm, a chromatic aberration of 1.5 mm, a focal spread of 2.5 nm and a convergence angle of 0.1 mrad. The relaxed atomic configuration is obtained using DFT simulations. Our experimental data agree well with the simulated results when the defocus is –9 nm. Gaussian blur was applied to all HRTEM images in Figure 1 - 5 in order to reduce the pixel noise.

DFT Simulations. Our first-principles calculations are all performed using the Quantum-Espresso code [3] under the framework of density functional theory.[4] RRKJ type ultra-soft pseudo-potentials[5] are employed together with the generalized gradient approximation in the Perdew, Burke, and Ernzerhof parametrization.[6] The plane wave cutoff energy is 40 Ry. The estimated self-consistency energy error is less than 10^{-8} Ry. The structure is relaxed until the total energy change is less than 10^{-4} Ry and the components of the forces are smaller than 10^{-3} Ry/Bohr. We use an interlayer spacing of 10 Å to avoid artifacts of the weak van der Waals interaction. The energy barriers were calculated by the nudged elastic band (NEB) method.[7]

Edge trapped Pt atoms

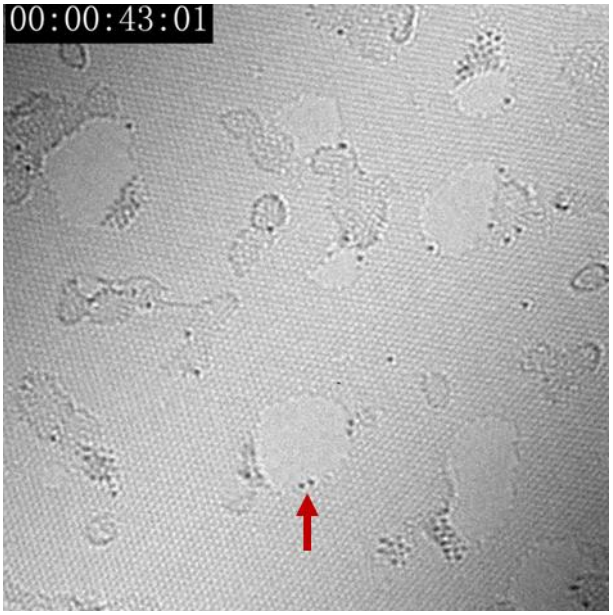

(a)

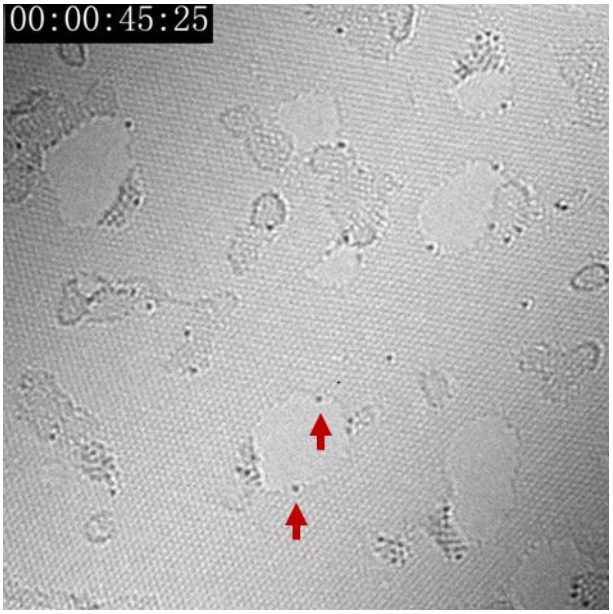

(b)

Figure S1. Video frames decoded from a movie. (a) The arrow indicates two neighboring Pt atoms; (b) They are separated in a few seconds.

Analysis of the knock-on displacement rate and the temperature effect

The displacement rate can be estimated as $p = \sigma_{tot} \times j$ with σ_{tot} being the total scattering cross section and j the beam intensity. The calculated cross sections are plotted in Figure S4 (a). Increasing the atomic number from carbon to gold can increase the cross section by a factor of ~ 100. The approximate rate is about 10 events per second for Au while 0.1 events per second under the imaging condition.

Figure S4 (b) shows the curves of transferred energy versus recoil angles. The average transferred energy can be estimated by

$$T_{ave} = \frac{1}{\sigma_{tot}} \int_{\pi}^{\theta_0} T_{max} \sin^2 \frac{\theta}{2} \frac{d\sigma_R}{d\theta} d\theta \quad \text{(S1)}$$

where θ_0 is the screening angle and $\frac{d\sigma_R}{d\theta}$ the differential Rutherford scattering cross section per recoil angle[8]

$$\theta_0 = 0.117 \frac{Z^{1/3}}{E_0^{1/2}} \quad \text{(S2)}$$

$$\frac{d\sigma_R}{d\theta} = \frac{\pi^2}{90} \sin\theta \frac{d\sigma_R}{d\Omega} \quad \text{(S3)}$$

$$\frac{d\sigma_R}{d\Omega} = \frac{Z^2 e^4 \left(1-\beta^2\right)}{m^2 c^4 \beta^2} \sin^{-4} \frac{\theta}{2} \quad \text{(S4)}$$

The parameters in the above equations are listed below:

$\frac{d\sigma_R}{d\Omega}$: The differential Rutherford scattering cross section per solid angle

Z: Atomic number of the target nucleus

E_0 (= 60 keV): The electron energy

e: Electron charge

m: Electron mass

c: The velocity of light

β: A correction coefficient given by $\beta^2 = \frac{E_0\left(E_0 + 2mc^2\right)}{\left(E_0 + mc^2\right)^2}$

After integrating Equation (S1), a simple formula is obtained:

$$\frac{T_{\text{ave}}}{T_{\text{max}}} = \left(\frac{\theta_0}{2}\right)^2 \ln\left(\frac{2}{\theta_0}\right)^2 \tag{S5}$$

For Au, T_{ave} = 5 meV; For C, T_{ave} = 18 meV. Considering the high thermal conductivity of graphene and low collision frequency, the temperature rise is negligible.

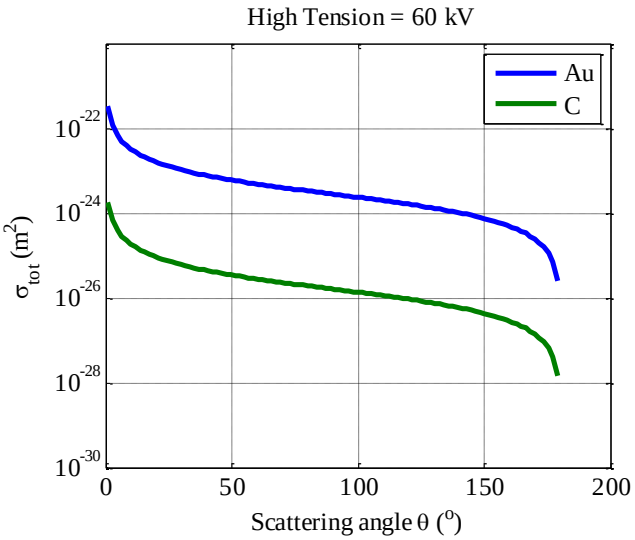

(a)

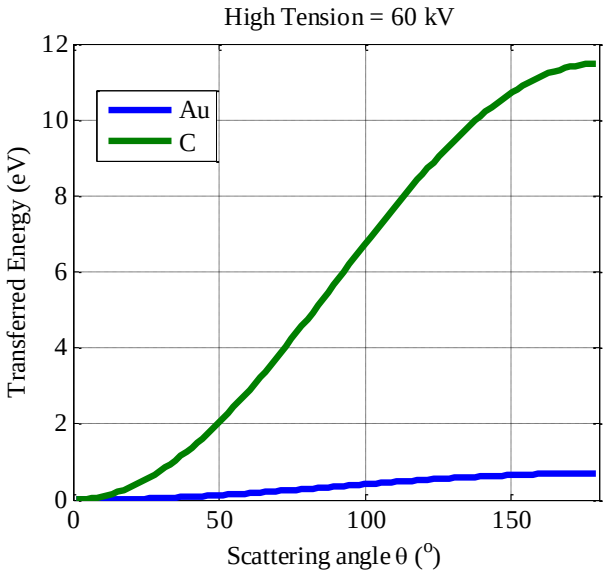

(b)

Figure S2. (a) The cross section versus scattering angle; (b) The transferred energy versus scattering angle.

Snapshots of all observed configurations extracted from Movie S1

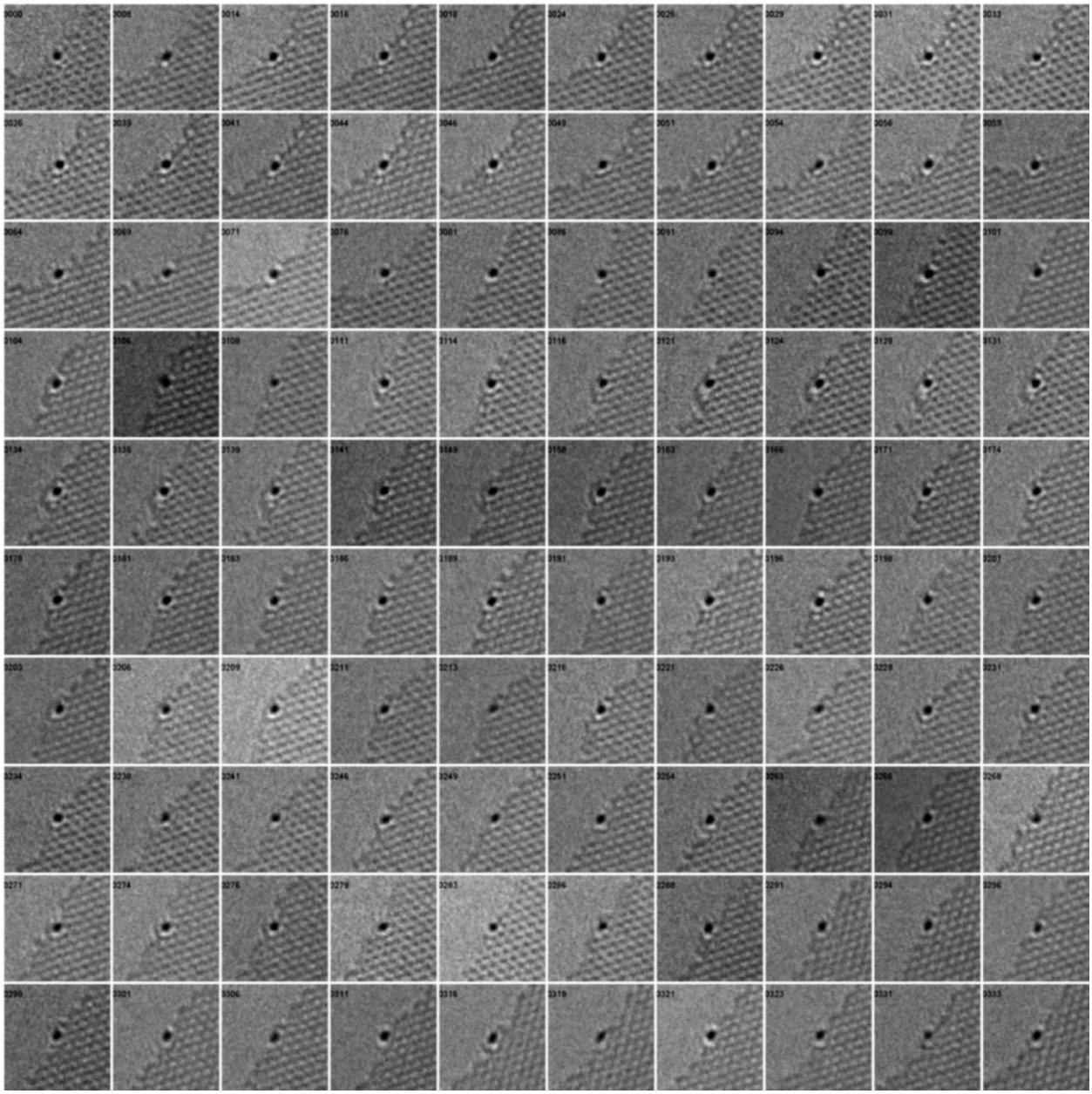

(a)

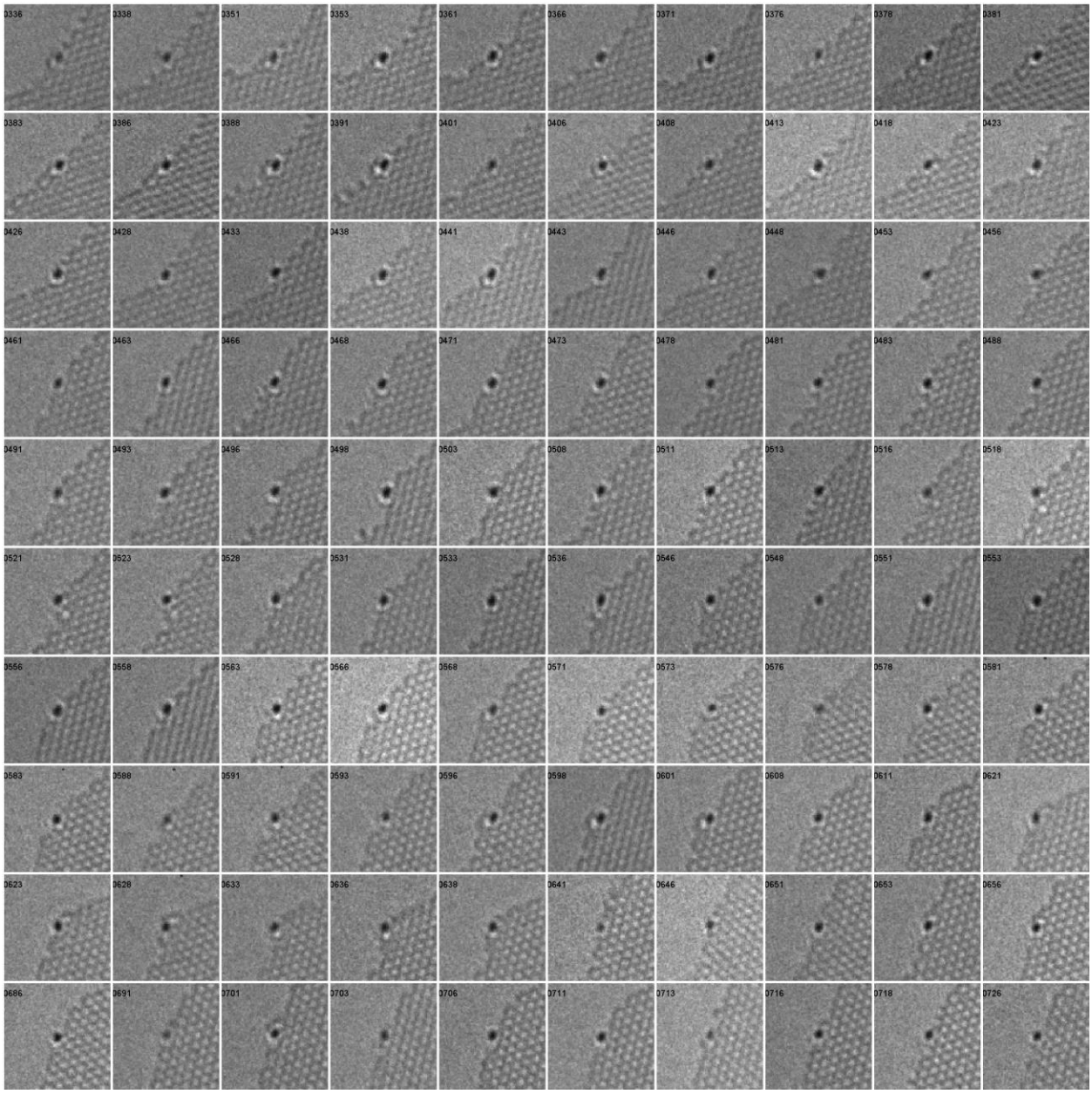

(b)

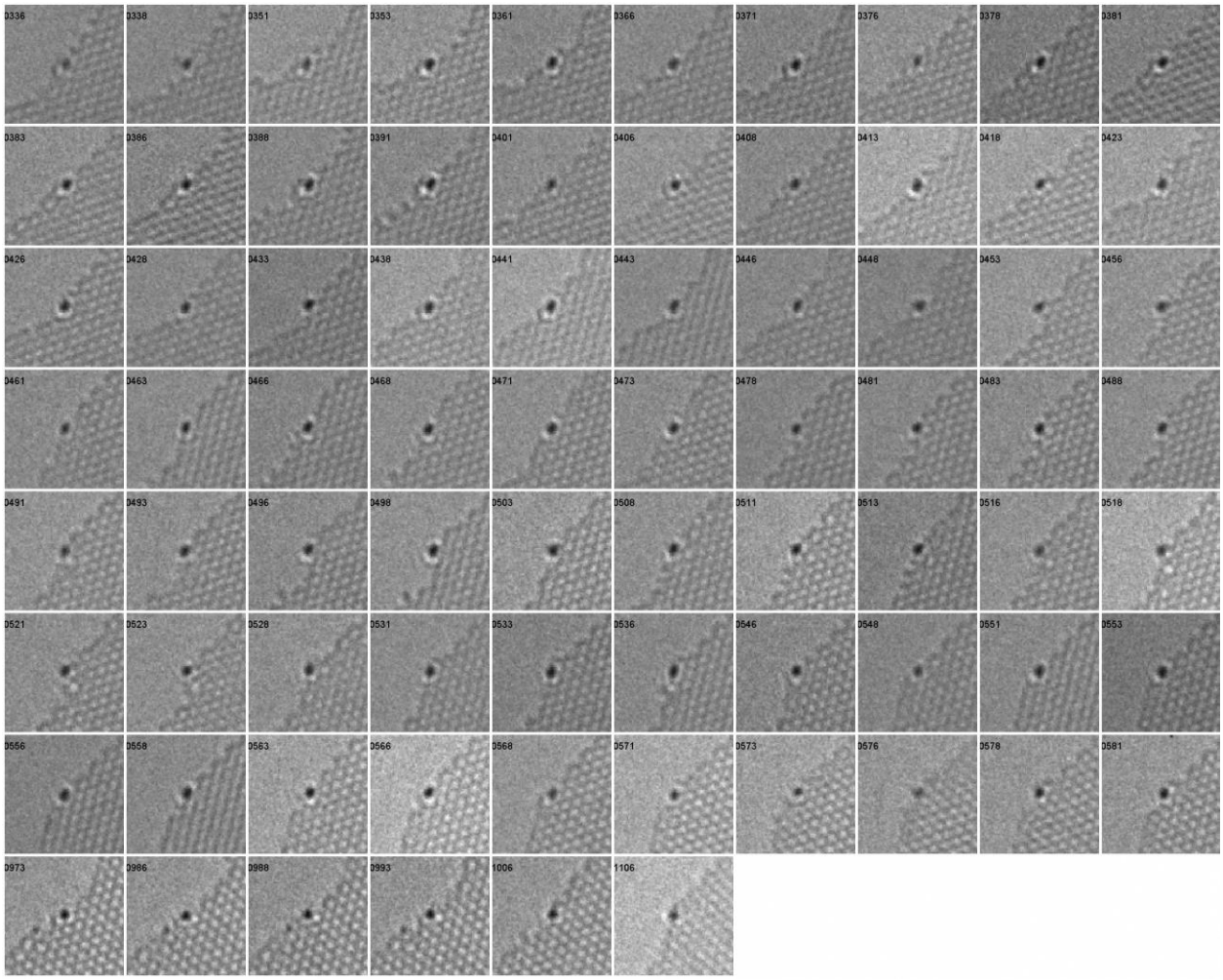

(c)

Figure S3. (a-c) All snapshots of the configurations extracted from Movie S1. The label inside each small figure is the corresponding time.

References

1. X. S. Li, W. W. Cai, J. H. An, S. Kim, J. Nah, D. X. Yang, R. Piner, A. Velamakanni, I. Jung, E. Tutuc, S. K. Banerjee, L. Colombo and R. S. Ruoff, *Science*, 2009, **324**, 1312-1314.

2. W. Regan, N. Alem, B. Aleman, B. Geng, C. Girit, L. Maserati, F. Wang, M. Crommie and A. Zettl, *Appl. Phys. Lett.*, 2010, **96**, 113102-113103.

3. P. Giannozzi, S. Baroni, N. Bonini, M. Calandra, R. Car, C. Cavazzoni, D. Ceresoli, G. L. Chiarotti, M. Cococcioni, I. Dabo, A. Dal Corso, S. de Gironcoli, S. Fabris, G. Fratesi, R. Gebauer, U. Gerstmann, C. Gougoussis, A. Kokalj, M. Lazzeri, L. Martin-Samos, N. Marzari, F. Mauri, R. Mazzarello, S. Paolini, A. Pasquarello, L. Paulatto, C. Sbraccia, S. Scandolo, G. Sclauzero, A. P.

Seitsonen, A. Smogunov, P. Umari and R. M. Wentzcovitch, *J. Phys.: Condens. Matter*, 2009, **21**, 395502.

4. S. Baroni, S. de Gironcoli, A. Dal Corso and P. Giannozzi, *Rev. Mod. Phys.*, 2001, **73**, 515-562.

5. A. M. Rappe, K. M. Rabe, E. Kaxiras and J. D. Joannopoulos, *Phys. Rev. B*, 1990, **41**, 1227-1230.

6. J. P. Perdew, K. Burke and M. Ernzerhof, *Phys. Rev. Lett.*, 1996, **77**, 3865-3868.

7. G. Henkelman, *J. Chem. Phys.*, 2000, **113**, 9901.

8. M. Kiritani, *Journal of the Physical Society of Japan*, 1976, **40**, 1035.